Precision Spectroscopy with Entangled States: Measurement of Electric Quadrupole Moments

C. F. Roos[*,†], M. Chwalla[*], K. Kim[*], M. Riebe[*] and R. Blatt[*,†]

[*]*Institut für Experimentalphysik, Universität Innsbruck, Technikerstr. 25, A-6020 Innsbruck, Austria*
[†]*Institut für Quantenoptik und Quanteninformation, Österreichische Akademie der Wissenschaften, Otto-Hittmair-Platz 1, A-6020 Innsbruck, Austria*

Abstract. Entangled states of atoms prepared in a decoherence-free subspace are shown to be useful for precision spectroscopy. Energy level shifts can be measured by using a pair of atoms in a Bell state for performing phase-estimation by generalized Ramsey experiments. The immunity of decoherence-free subspaces against certain sources of noise allows for long excitation times in the presence of noise that would render single-atom experiments impossible. We employ this technique for a measurement of the electric quadrupole moment Θ of the meta-stable $3D_{5/2}$ level of $^{40}Ca^{+}$ which is found to be $\Theta(3d,5/2) = 1.83(1)ea_0^2$.

Keywords: Entanglement, precision spectroscopy, trapped ions, quadrupole moment
PACS: 3.65.Ud, 3.67.-a, 32.10Dk, 42.62.Fi

INTRODUCTION

Entanglement has been recognized as a key resource for quantum computation[1] and quantum cryptography[2] in the last couple of years. For quantum metrology, use of entangled states has been mainly discussed as a means of improving the signal-to-noise ratio[3, 4, 5] and first demonstration experiments were performed[6]. In addition, entangled states were used in experiments for efficient quantum state detection[7] and the measurement of scattering lengths[8]. In quantum information processing, decoherence-free subspaces[9] protect quantum information against detrimental influences from a decohering environment[10] and yield significantly enhanced coherence times[11]. This property makes spectroscopy in decoherence-free subspaces attractive as long measurement times can be used[12].

Ramsey's interferometric technique[13] of measuring transition frequencies by monitoring the evolution of the relative phase of a superposition state of atomic energy levels can be generalized[5] to maximally entangled states: The two-atom state $\Psi = \frac{1}{\sqrt{2}}(|u_1\rangle|u_2\rangle + |v_1\rangle|v_2\rangle)$ evolves for a duration τ under free precession into the state $\Psi(\tau) = \frac{1}{\sqrt{2}}(|u_1\rangle|u_2\rangle + \exp(i\phi(\tau))|v_1\rangle|v_2\rangle)$ where $\phi(\tau) = \tau/\hbar[(E_{u_1}+E_{u_2}) - (E_{v_1}+E_{v_2})]$ is proportional to the differences in atomic energies E_{u_k}, E_{v_k} of the involved levels. The real part $\cos\phi(\tau)$ of the phase factor is determined by projecting the atoms onto the states $|\pm\rangle_k = \frac{1}{\sqrt{2}}(|u_k\rangle \pm |v_k\rangle)$ and measuring the quantum correlations $\sigma_x^{(1)} \otimes \sigma_x^{(2)}$ where $\sigma_x^{(k)} = |+\rangle\langle+|_k - |-\rangle\langle-|_k$. If Ψ is an element of a decoherence-free subspace, free precession times τ of several seconds[14, 15] allow for highly accurate phase estimation.

MEASUREMENT OF ELECTRICAL QUADRUPOLE MOMENTS

In atomic optical frequency standards based on single trapped ions[16] having one valence electron, the transition frequency from the S ground state to a metastable D_j state is measured by an optical frequency comb. The D_j state's atomic electric quadrupole moment interacting with residual electric quadrupole fields[17] gives rise to energy level shifts that are typically on the order of a few Hertz. The shift of the Zeeman sublevel $|D_j, m_j\rangle$ in a quadrupole field $\Phi(x,y,z) = A(x^2+y^2-2z^2)$ is given by

$$\hbar\Delta\nu = \frac{1}{4}\frac{dE_z}{dz}\Theta(D,j)\frac{j(j+1)-3{m_j}^2}{j(2j-1)}(3\cos^2\beta - 1), \qquad (1)$$

where $dE_z/dz = 4A$ is the electric field gradient along the potential's symmetry axis z, β denotes the angle between the quantization axis z and $\Theta(D,j)$ expresses the strength of the quadrupole moment in terms of a reduced matrix element[17].

Recently, quadrupole moments have been measured for metastable states of $^{88}Sr^+$, $^{199}Hg^+$ and $^{171}Yb^+$ with a precision ranging from about 4% to 12% (refs. [18, 19, 20]). In these single-ion experiments, narrow-linewidth lasers are employed to detect electric quadrupole shifts by measuring the transition frequency from the electronic ground state to the metastable state. Alternatively, the quadrupole shift could also be measured by performing Ramsey experiments with an ion prepared in a superpositions of Zeeman D_j sublevels. Both measurement schemes are subject to phase decoherence. Laser frequency noise limits the coherence time if the S state is used as the reference state. Magnetic field noise giving rise to first-order Zeeman shifts renders the measurement scheme based on D state superpositions difficult. Both sources of phase noise may be eliminated by replacing the single ion by a two-ion entangled state prepared in a decoherence-free subspace[12]. The phase of the two-ion Bell state $\Psi = \frac{1}{\sqrt{2}}(|m_1\rangle|m_2\rangle + |m_3\rangle|m_4\rangle)$, where $|m_i\rangle \equiv |D_j, m_i\rangle$ and the magnetic quantum numbers m_i satisfy $m_1 + m_2 = m_3 + m_4$, is not affected by fluctuations of the magnetic field to first order since both parts of the superposition are Zeeman-shifted by the same amount (see Fig. 1c). Also, frequency noise of the laser used for preparing Ψ is relevant only during the comparatively short state preparation and read-out steps but not during the long interrogation period. For suitably chosen values of $m_1, \ldots m_4$, a decoherence-immune state can be prepared that is sensitive to the electric quadrupole shift as will be shown below (see also Fig. 1b). Measuring the Bell state's phase evolution in a Ramsey experiment yields information about the magnitude of the shift[21].

EXPERIMENTAL SETUP

The isotope $^{40}Ca^+$ has a single valence electron and no hyperfine structure (Fig. 1a). For its metastable $3d\,^2D_{5/2}$ state (lifetime $\tau_{D_{5/2}} = 1.168(7)$ s), a quadrupole moment of $1.917\,ea_0^2$ was calculated[22, 23]. For the experiment, two $^{40}Ca^+$ ions are trapped along the axis of a linear ion trap. By applying a static (dc) voltage ranging from 500 to 2000 V to the tip electrodes[24], axial center-of-mass (COM) mode trap frequencies ω_z ranging from 850 to 1700 kHz are achieved. A CCD camera images the ions' fluorescence. The

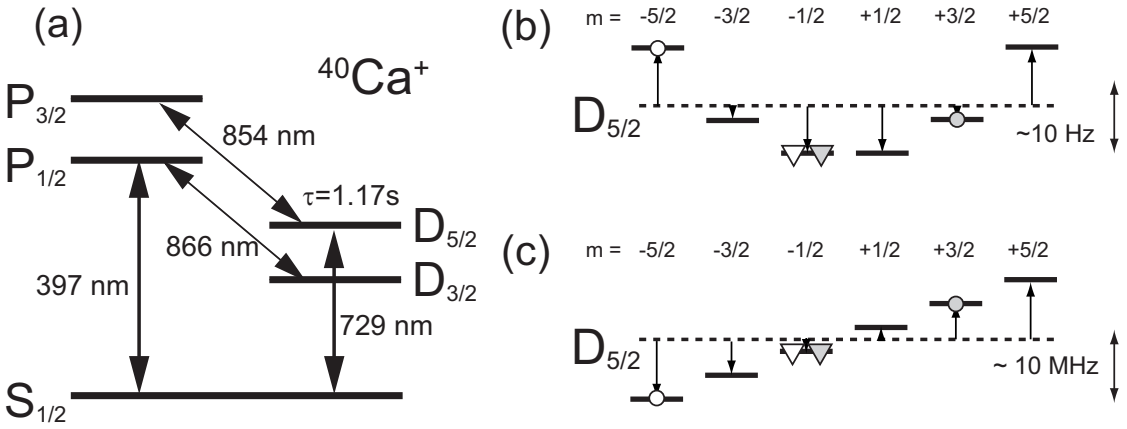

FIGURE 1. (a) Relevant atomic levels of $^{40}Ca^+$. Bell states are prepared by coherently exciting the $S_{1/2} \leftrightarrow D_{5/2}$ quadrupole transition. The $S_{1/2} \leftrightarrow P_{1/2}$ is used for quantum state read-out, lasers at 866 and 854 serve as repumping and quenching lasers. (b) Energy level shift caused by an electric quadrupole potential. Energy levels occurring in the state $\Psi_D = \frac{1}{\sqrt{2}}(|\circ\rangle|\bullet\rangle + |\triangledown\rangle|\blacktriangledown\rangle)$ (eq. (2)) are denoted by the symbols $\circ, \triangledown, \bullet, \blacktriangledown$, the open (filled) symbols corresponding to levels occupied by atom 1 (2), respectively. The combined Zeeman energy of the $|\circ\rangle|\bullet\rangle$-states equals the energy of the $|\triangledown\rangle|\blacktriangledown\rangle$-states, making Ψ_1 immune against magnetic field noise. Since an electric quadrupole field shifts the $|\circ\rangle|\bullet\rangle$- and $|\triangledown\rangle|\blacktriangledown\rangle$-states in opposite directions, Ψ_1 is suitable for a measurement of the quadrupole shift. (c) Energy level shift of the $|m\rangle \equiv |D_{5/2}, m\rangle$ states in a weak magnetic field. In the experiment, the Zeeman shift is typically five orders of magnitude bigger than the quadrupole shift.

degeneracy of the Zeeman states is lifted by applying a magnetic bias field of 2.9 G. The ions are cooled to the ground state of the axial COM mode by Doppler and sideband cooling[25]. For coherent quantum state manipulation, the ions are individually excited on the $|S\rangle \equiv S_{1/2}(m=-1/2) \leftrightarrow |D\rangle \equiv D_{5/2}(m=-1/2)$ transition by a tightly focussed laser beam (laser linewidth ≈ 150 Hz) resonant with either the carrier transition or the upper motional sideband of the COM mode. A detailed description of the experimental setup can be found in ref.[24].

The Bell state $\Psi_{SD}^{\pm} = (|S\rangle|D\rangle \pm |D\rangle|S\rangle)/\sqrt{2}$ is created with a fidelity of about 90% by a sequence of three laser pulses[11]. Additional carrier π pulses transfer the entanglement from Ψ_{SD}^{+} into the $D_{5/2}$ Zeeman state manifold, thus generating the state

$$\Psi_D = \frac{1}{\sqrt{2}}(|-5/2\rangle|+3/2\rangle + |-1/2\rangle|-1/2\rangle). \qquad (2)$$

This magnetic field-insensitive state is used for a measurement of the quadrupole shift. The state Ψ_D is slightly less sensitive to the quadrupole shift than the state $|-5/2\rangle|+5/2\rangle + |-1/2\rangle|+1/2\rangle$ but has the advantage of being easier to produce starting from state Ψ_{SD}^{+}. In the vicinity of the trap center, the dc voltage applied to the tip electrodes creates a rotationally symmetric electric quadrupole potential Φ_{tips} which shifts the energy of the constituents of the superposition state Ψ_1 by $\hbar\Delta_1 = 24/5\,\hbar\delta$ with respect to each other. Here, $\hbar\delta$ is the shift that a single ion in state $|-5/2\rangle$ would experience. The two-ion shift is bigger by $12/5$ because two ions contribute that are prepared in substates which shift in opposite directions. In addition, the second ion's Coulomb field doubles

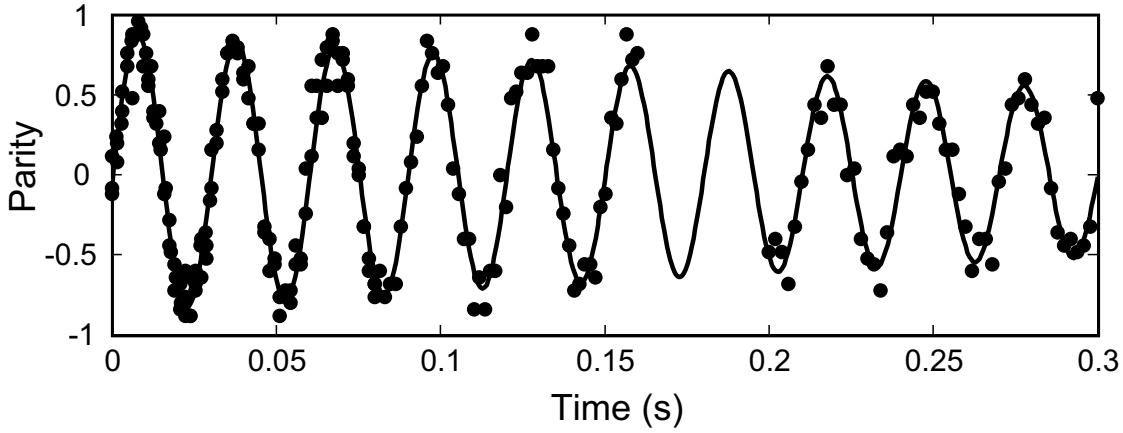

FIGURE 2. Parity oscillations of the entangled state Ψ_D at $U_{tips} = 750$ V tip voltage. The experiment is repeated 100 times for each data point. An exponentially damped sinusoidal function is fitted to the data. For Ψ_D, the oscillation frequency is $\Delta = (2\pi)\,33.35(3)$ Hz and the damping time $587(70)$ ms. For the plot, five different data sets were merged. No data were taken covering waiting times around 170 ms. To exclude slow drifts of the initial parity over time, data for waiting times up to 20 ms were repeatedly taken.

the electric field gradient at the location of the other ion[12]. For the shift measurement, Ψ_D is let to evolve into $\Psi_D(\tau) = \frac{1}{\sqrt{2}}(|-5/2\rangle|+3/2\rangle + \exp(i\Delta_1\tau)|-1/2\rangle|-1/2\rangle)$ and $\cos(\Delta\tau)$ is measured for τ ranging from 0 to 300 ms.

Figure 2a shows the resulting parity oscillations[11] at a frequency $\Delta = (2\pi)\,33.35(3)$ Hz. Disentanglement of $\Psi_D(\tau)$ by spontaneous decay manifests itself as damping of the oscillations with a damping time constant $\tau_d = 587(70)$ ms close to the expected value $\frac{1}{2}\tau_{D_{5/2}} = 584$ ms. The parity oscillation frequency is mainly due to the electric quadrupole shift. A magnetic field gradient in the direction of the ion crystal can give rise to an additional contribution[12]. This unwanted term can be cancelled by repeating the experiment with a quantum state where ions 1 and 2 exchange their role[21].

MEASUREMENT OF THE $D_{5/2}$ QUADRUPOLE MOMENT

The rotationally symmetric quadrupole field Φ_{tips} created by the static tip voltages U_{tips} is calibrated by measuring the ion's axial oscillation frequency ω_z. By recording parity oscillations at different tip voltages, we measure the quadrupole shift $\Delta/(2\pi)$ as a function of the electric field gradient and observe a linear change in $\Delta(U_{tips})$. For a precise determination of the quadrupole moment, the dependence of the quadrupole shift on the orientation of the magnetic field should be minimized by aligning the field with a prinicipal axis of $U_{tips}(\mathbf{r})$. We investigate the angle dependence of Δ by varying the orientation of the magnetic field in a plane that also contains the z-axis of the trap. The magnetic field $\vec{B}$ is set by passing currents I_{h_1}, I_{h_2}, I_v through three mutually orthogonal pairs of coils (see Fig. 3 a). We calibrate the field coils and null the offset fields by measuring the Zeeman shift of the $|S_{1/2}, m = -1/2\rangle \leftrightarrow |D_{5/2}, m = -1/2\rangle$ transition as

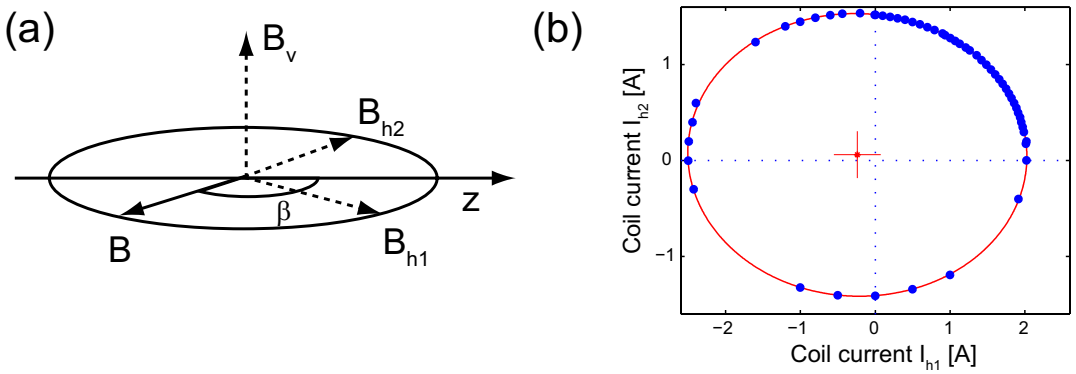

FIGURE 3. (a) Geometry of magnetic field coils. The angle β is varied by appropriately changing the current in pairs of coils producing the magnetic fields B_{h1}, B_{h2}. Field B_v is used to null residual fields in the perpendicular direction. (b) Coil currents (I_{h_1}, I_{h_2}) that yield a constant Zeeman shift. A determination of the principle axes of the ellipse yields the proportionality constants between currents and the produced fields. The shift of the ellipse from the center is caused by residual magnetic fields.

a function of the currents. We estimate that the offset fields can be zeroed to a value below 1% of the applied bias field. After nulling the field in the v-direction, we map out the values of (I_{h_1}, I_{h_2}) that yield a constant Zeeman shift and fit an ellipse to the data (see Fig. 3 b). These current values rotate $\vec{B}$ in a horizontal plane that also contains the symmetry axis (z) of the ion trap. A similar procedure is applied for calibrating the v-coil.

Initialization of the ions in a pure state prior to coherent manipulation requires optical pumping. The standard technique of optical pumping by a circularly polarized laser beam oriented along the direction of the magnetic field cannot be used as the latter is continuously varied. Instead, we perform frequency-resolved optical pumping on the quadrupole transition. Due to the magnetic bias field lifting the energy degeneracy or the Zeeman states, the ions can be prepared in the $|S_{1/2}, m = -1/2\rangle$ state for an arbitrary orientation of the magnetic field by optical pumping on the quadrupole transition. For this, the $|S_{1/2}, m = +1/2\rangle \leftrightarrow |D_{5/2}, m = -3/2\rangle$ transition is excited while the repumping lasers on the $D_{5/2} \leftrightarrow P_{3/2}$ and $D_{3/2} \leftrightarrow P_{1/2}$ transitions are switched on at the same time. After an excitation of 1 ms duration, at least 99.9% of the population has been pumped to the $|S_{1/2}, m = -1/2\rangle$ state. This method of optical pumping has the advantage of being not only insensitive to the orientation of the pumping beam but also to its polarization.

Figure 4 shows the dependence of the electric quadrupole shift on the orientation of the magnetic field. The measurement shows the sinusoidal variation of Δ measured at $U_{tips} = 1000$ V as a function of field angle β. Generally, it cannot be excluded that the quadrupole field has imperfect rotational symmetry. In this case, the factor $(3\cos^2(\beta) - 1)$ in eq.(1) needs to be replaced by $(3\cos^2\beta - 1) - \varepsilon \sin^2\beta \cos(2\alpha)$ where ε characterizes the asymmetry and α its direction[17]. Note, however, that the additional term vanishes for $\beta = 0$. At the angle that maximizes Δ, another maximization is performed in the perpendicular direction to determine the direction corresponding to $\beta = 0$. Figure 5a displays the quadrupole shift measured at $\beta = 0$ as a function of the

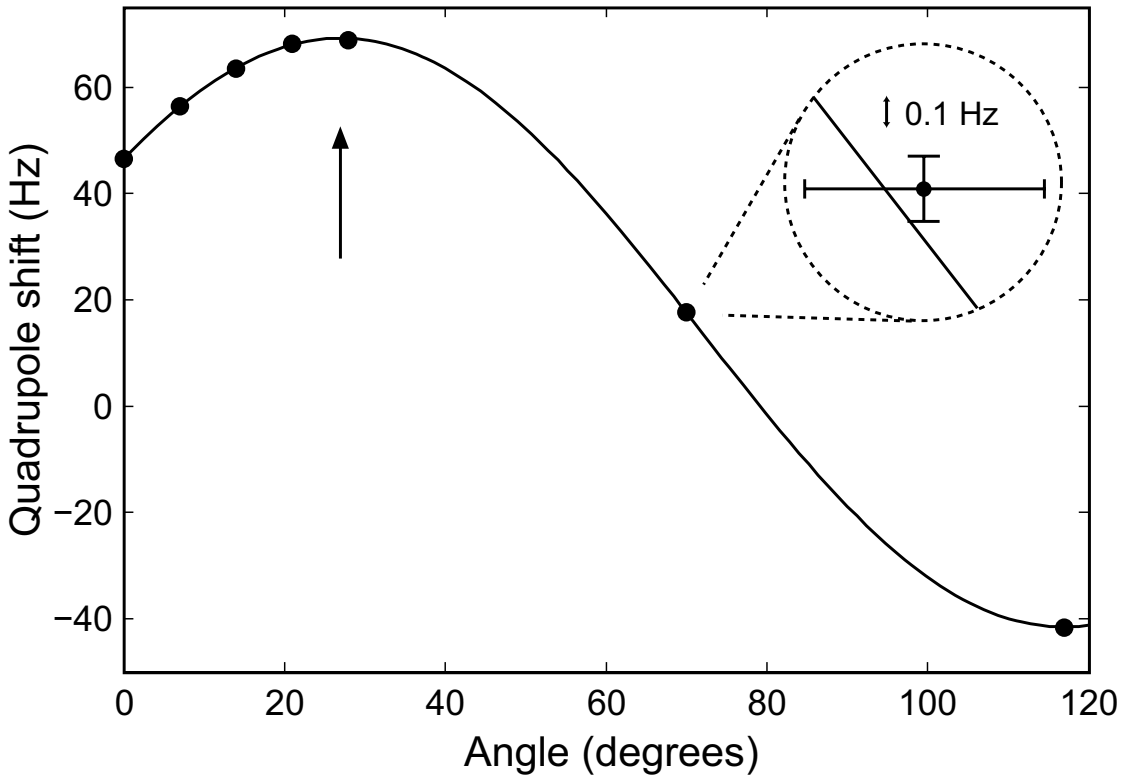

FIGURE 4. Angular dependence of the quadrupole shift. Quadrupole shift $\Delta/(2\pi)$ at $U_{tips} = 1000$ V as a function of the magnetic field orientation $\beta - \beta_0$. The data are fitted by $\Delta = \Delta_a + \Delta_b \cos^2(\beta - \beta_0)$, yielding $\beta_0 = 26.9°$. The arrow indicates the angle corresponding to $\beta = 0$. For the determination of the quadrupole moment, shift measurements are performed at $\beta = 0$ since errors in β enter the calculation only in second order. Note that the error bars are smaller than the point size. The inset in the upper right corner shows an enlarged data point.

electric field gradient dE_z/dz. Using $dE_z/dz = -m\omega_z^2/e$, the gradient is calibrated by a measurement of the ion's oscillation frequency ω_z. By fitting a straight line $\Delta/(2\pi) = \Delta_0/(2\pi) + a\frac{dE_z}{dz}$ to the data, we determine the slope $a = 2.975(2)$ Hz mm^2/V and the offset $\Delta_0/(2\pi) = -2.4(1)$ Hz. The major part of the phase oscillation frequency Δ_0 at $\frac{dE_z}{dz} = 0$ is caused by the second-order Zeeman effect that contributes $\Delta_{B^2}/(2\pi) = -2.9$ Hz at the bias field of 2.9 G. The remaining part $\Delta_0 - \Delta_{B^2}$ is attributed to a residual quadrupole field caused by stray charges. The quadrupole moment $\Theta(3d, 5/2) = \frac{5}{12}ha$ is proportional to the slope a. While the uncertainty in the value of a is smaller than 10^{-3}, the main uncertainty in $\Theta(3d, 5/2)$ is due to errors in the determination of the angle β. Assuming that the angle can be determined with an accuracy of 3 degrees, we determine the quadrupole moment to be $\Theta(3d, 5/2) = 1.83(1)\mathrm{ea}_0^2$.

Errors in the measurement of the angle β are caused by the electric potential Φ_s of stray charges. Maximizing the the quadrupole shift by varying the direction of the magnetic field $\vec{B}$ then aligns the field with a principal axis of the quadrupolar part of $\Phi_{tips} + \Phi_s$ instead of Φ_{tips}. However, it is possible to place upper bounds on the

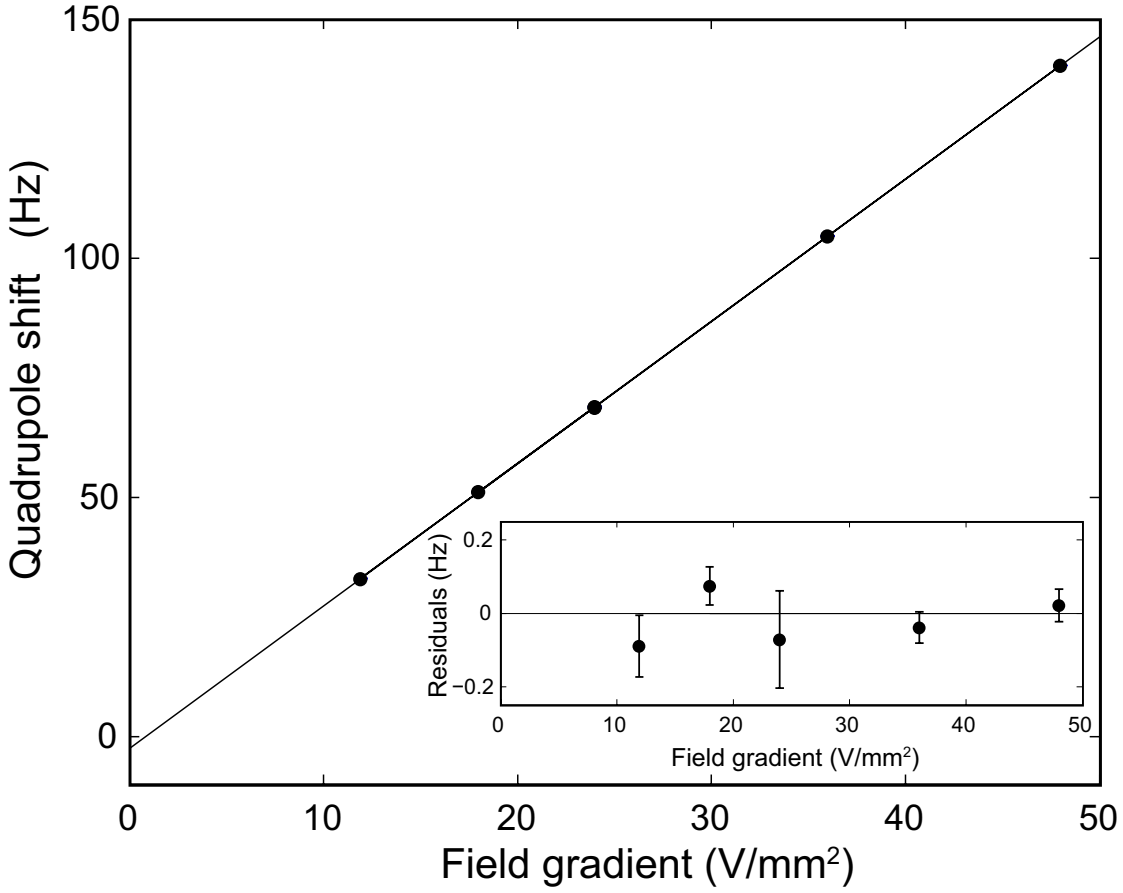

FIGURE 5. Quadrupole shift as a function of the applied external electric field gradient dE_z/dz. The offset at $dE_z/dz = 0$ is mainly due to the second-order Zeeman effect. The quadrupole moment is proportional to the slope which is measured with an uncertainty of less than 0.1%. The inset shows the deviation of the data points from the linear fit.

magnitude of the possible misalignment[21]. Further sources of errors we considered are errors in the calibration of the field gradient strength by measuring the ions' oscillation frequency ω_z. Here, ac-field along the trap axis could affect the calibration. Shifts caused by the tensor part of ac-Stark shifts[17] of the $D_{5/2}$ state are expected to be negligible.

CONCLUSION

These results show the viability of the approach of designing specific entangled states for precision measurements. For frequency standard applications, minimization of the quadrupole shift is imperative[26, 27]. Note that, by using designed entangled states, the quadrupole shift could be cancelled by averaging the results over states with different magnetic quantum numbers[12]. While previously the use of entangled states was to enhance the signal-to-noise ratio, the use of a designed pair of entangled ions allows an atomic clock measurement to be performed in a subspace free of magnetic field

noise. This is achieved with unprecedented precision on an even isotope which opens the perspective for optical frequency standards based on a whole variety of easily accessible atomic systems not considered so far.

ACKNOWLEDGMENTS

We thank H. Häffner for his contributions to the optical pumping scheme and acknowledge help with the experiment from T. Körber, W. Hänsel, D. Chek-al-kar, M. Mukherjee, and P. Schmidt. We gratefully acknowledge support by the Austrian Science Fund (FWF), by the European Commission (SCALA, CONQUEST networks), and by the Institut für Quanteninformation GmbH. This material is based upon work supported in part by the U. S. Army Research Office.

REFERENCES

1. M. A. Nielsen, and I. L. Chuang, *Quantum computation and quantum information*, Cambridge Univ. Press, Cambridge, 2000.
2. N. Gisin, G. Ribordy, W. Tittel, and H. Zbinden, *Rev. Mod. Phys.* **74**, 145–195 (2002).
3. V. Giovannetti, S. Loyd, and L. Maccone, *Science* **306**, 1330–1336 (2004).
4. V. Giovannetti, S. Loyd, and L. Maccone, *Phys. Rev. Lett.* **96**, 010401 (2006).
5. J. J. Bollinger, W. M. Itano, D. J. Wineland, and D. J. Heinzen, *Phys. Rev. A* **54**, R4649–4652 (1996).
6. D. Leibfried *et al.*, *Science* **304**, 1476–1478 (2004).
7. P. O. Schmidt, T. Rosenband, C. Langer, W. M. Itano, J. C. Bergquist, and D. J. Wineland, *Science* **309**, 749–752 (2005).
8. A. Widera *et al.*, *Phys. Rev. Lett.* **92**, 160406 (2004).
9. D. A. Lidar, I. L. Chuang, and K. B. Whaley, *Phys. Rev. Lett.* **81**, 2594–2597 (1998).
10. D. Kielpinski *et al.*, *Science* **291**, 1013–1015 (2001).
11. C. F. Roos *et al.*, *Phys. Rev. Lett.* **92**, 220402 (2004).
12. C. F. Roos, *arXiv*:quant-ph/0508148 (2005).
13. N. F. Ramsey, *Phys. Rev.* **78**, 695–699 (1950).
14. H. Häffner *et al.*, *Appl. Phys. B* **81**, 151–153 (2005).
15. C. Langer *et al.*, *Phys. Rev. Lett.* **95**, 060502 (2005).
16. A. A. Madej, and J. E. Bernard, "Single-ion optical frequency standards", in *Frequency measurement and control*, edited by A. N. Luiten, *Topics. Appl. Phys.* **79**, 153–195 (2001).
17. W. M. Itano, *J. Res. Natl. Inst. Stand. Technol.* **105**, 829–837 (2000).
18. W. H. Oskay, W. M. Itano, and J. C. Bergquist, *Phys. Rev. Lett.* **94**, 163001 (2005).
19. G. P. Barwood, H. S. Margolis, G. Huang, P. Gill, and H. A. Klein, *Phys. Rev. Lett.* **93**, 133001 (2004).
20. T. Schneider, E. Peik, and Chr. Tamm, *Phys. Rev. Lett.* **94**, 230801 (2005).
21. C. F. Roos, M. Chwalla, K. Kim, M. Riebe, and R. Blatt, *Nature* **443**, 316–319 (2006).
22. W. M. Itano, *Phys. Rev. A* **73**, 022510 (2006).
23. C. Sur *et al.*, *Phys. Rev. Lett.* **96**, 193001 (2006).
24. F. Schmidt-Kaler *et al.*, *Appl. Phys. B* **77**, 789–796 (2003).
25. Ch. Roos *et al.*, *Phys. Rev. Lett.* **83**, 4713–4716 (1999).
26. H. S. Margolis *et al. Science* **306**, 1355–1358 (2004).
27. P. Dubé *et al.*, *Phys. Rev. Lett.* **95**, 033001 (2005).